Vessel Velocity Estimation and Tracking From Doppler Echoes of T/R-R Composite Compact HFSWR

Weifeng Sun, *Member, IEEE*, Zhenzhen Pang, Weimin Huang, *Senior Member, IEEE*, Yonggang Ji, *Member, IEEE*, and Yongshou Dai

***Abstract*—Vessel speed and heading are two important kinematic parameters describing its state of motion. However, due to low spatial resolution of a compact high-frequency surface wave radar (HFSWR), vessel speed and heading cannot always be accurately estimated. Since HFSWR can measure vessel Doppler velocity with relatively high accuracy, it is possible to estimate a vessel's vector velocity based on two Doppler velocities measured along two different directions. In this article, a newly developed T/R-R composite compact HFSWR system is introduced, and a corresponding vessel velocity estimation method which employs a target's radial velocity and elliptical velocity, respectively, measured by the monostatic (T/R) and bistatic (T-R) settings is proposed. First, monostatic and bistatic tracks are independently generated using a multitarget tracking algorithm. Then, the obtained monostatic and bistatic tracks are matched using a track-to-track association method to determine the track pair belonging to each target. Subsequently, the associated track pairs are combined to produce fused tracks for improving positioning accuracy. Finally, vessel vector velocity is estimated based on the radial and elliptical velocities as well as the fused target position. Comparisons of vector velocity estimation results from radar field data with corresponding automatic identification system data demonstrate that the average root-mean-square-errors of the estimated speed and heading are 0.48 km/h and 3.9°, respectively, which meets the practical requirements of a maritime surveillance system. Moreover, the velocity estimation error is analyzed via theoretical derivation and experimental verification. The proposed method shows good potential in further improving the tracking accuracy.**

***Index Terms*—Compact high-frequency surface wave radar (HFSWR), T/R-R composite system, track association, track fusion, vector velocity estimation.**

Manuscript received January 3, 2021; revised March 20, 2021; accepted April 4, 2021. Date of publication April 7, 2021; date of current version May 10, 2021. This work was supported in part by the National Key R&D Program of China under Grant 2017YFC1405202, in part by the National Natural Science Foundation of China under Grant 62071493, Grant 61831010, and Grant 61671166, and in part by the Fundamental Research Funds for the Central Universities under Grant 19CX02046 A. *(Corresponding author: Weifeng Sun.)*

Weifeng Sun, Yonggang Ji, and Yongshou Dai are with the College of Oceanography and Space Informatics, China University of Petroleum (East China), Qingdao 266580, China (e-mail: sunwf@upc.edu.cn; jiyonggang@upc.edu.cn; daiys@upc.edu.cn).

Zhenzhen Pang is with the College of Control Science and Engineering, China University of Petroleum (East China), Qingdao 266580, China (e-mail: s19050022@s.upc.edu.cn).

Weimin Huang is with the Faculty of Engineering and Applied Science, Memorial University of Newfoundland, St. John's, NL A1B 3X5, Canada (e-mail: weimin@mun.ca).

Digital Object Identifier 10.1109/JSTARS.2021.3071625

I. Introduction

As an important over-the-horizon ocean remote sensing sensor for both wide-area sea state (current, wave, wind, etc.) inversion [1] and long-range sea-surface targets detection and tracking [2], [3], compact high-frequency surface wave radar (HFSWR) has raised significant interest in recent years for their deployment flexibility and less space requirement [4]. Several representative compact HFSWR systems have been developed, e.g., the SeaSonde system [5], [6], OSMAR-S system [7], [8], WERA-S system [9], CORMS system [10]–[12], etc. However, limited by the coarse bearing resolution due to reduced aperture size, compact HFSWR system operated in monostatic mode is difficult to provide accurate target position information. Plenty of research works have demonstrated the effectiveness of a bistatic HFSWR in both sea state estimation [13], [14] and target detection [15], but similar problems exist if a compact system is used.

In order to enhance the target detection performance of compact radar systems, networking observation becomes a feasible strategy and research focus [16], [17], but it brings an increase in system complexity and cost. To achieve a tradeoff between system performance and its complexity and cost, a T/R-R composite radar system consisting of a T/R monostatic radar and a T-R bistatic radar, as shown in Fig. 1, offers a new choice [18], [19] and can be regarded as the basic configuration of a networking system. For a T/R-R composite radar system, the T/R monostatic radar and T-R bistatic radar cooperatively illuminate targets within a common area simultaneously. As shown in Fig. 1, a target is observed by both the T/R monostatic radar and T-R bistatic radar. So far, very few T/R-R HFSWR systems have been developed and limited results have been reported [20]. In [15], analysis was only focused on target tracking performance of the T-R bistatic radar of a T/R-R system. Also, existing T/R-R studies mainly focus on theoretical and simulation analysis. In this article, a newly developed T/R-R composite compact HFSWR system is introduced, and a target vector velocity estimation method, which consists of a track association and fusion module and a vector velocity estimation module, is designed for such a system.

In an integrated maritime surveillance system, target speed and heading are of great importance. However, existing research works on target detection and tracking with HFSWR mainly

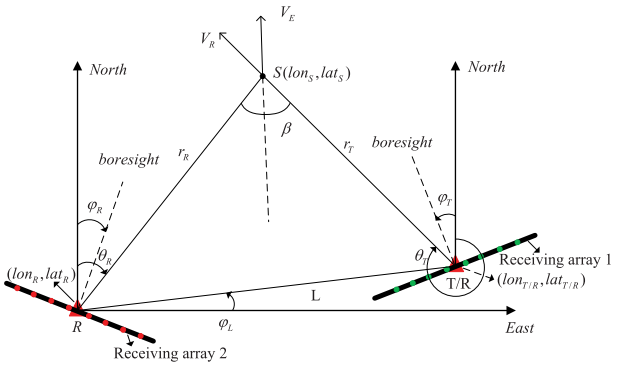

Fig. 1. Geometric configuration of a T/R-R composite radar system.

focus on enhancing the tracking performance in terms of improving bearing resolution [21], reducing track fragmentation [22], improving positioning accuracy [12], etc. Few studies have paid attention to estimating the target speed and heading [12], [23]. The traditional way to calculate these two parameters relies on target positions. Unfortunately, compact HFSWR can only provide coarse target positions due to its poor spatial resolution, thus, affecting target speed and heading estimation. As the monostatic radar and bistatic radar in a T/R-R composite system observe a target from different perspectives, the obtained redundant target location information may be combined via data association and fusion to improve the positioning accuracy. However, due to various kinds of interference, such as sea clutter [24], ionospheric clutter [25], radio frequency interference [26], etc., under a multitarget detection scenario, the data acquired by a compact HFSWR consist of multiple measurements (a.k.a. plots) of different targets and many false alarms due to interference. Therefore, it is challenging to identify the two measurements that are observed by two radars but belong to the same target just based on the data acquired at a single moment. Compared with a plot, a track connecting several plots sequentially better illustrate the motion characteristics of a target with higher certainty. Motivated by this consideration, first, target tracks can be separately generated by multitarget tracking algorithms [27] for both T/R monostatic radar and T-R bistatic radar. Then the monostatic and bistatic tracks can be compared and fused by track-to-track association and fusion methods to produce fused tracks with improved positioning accuracy.

So far, quite a few track-to-track association and fusion methods have been proposed. These track-to-track association methods can be classified into three categories. One includes statistical-based methods, such as the weighting method [28], joint probability data association (JPDA) method [29], multiple hypothesis tracking (MHT) method [30], etc. The second is fuzzy mathematics-based, such as the fuzzy mathematics-based clustering method [31]–[34], fuzzy double-threshold association algorithm [35], etc. The third type is artificial intelligence based, such as the neural network-based method [36], extreme learning machine-based method [37], etc. The track-to-track fusion algorithms include the covariance intersection (CI) method [38], the Bar-Shalom-Campo algorithm [39], adaptive track fusion approach with fuzzy computation [40], maximum a posterior probability-based state estimation fusion [41], etc. Track-to-track association and fusion methods are always applied sequentially, e.g., Singh and Sood [42] obtained the fused tracks with higher accuracy by joint probabilistic data association and neural network fusion algorithm for multiple maneuvering targets. It should be noted that only several representative track-to-track association and fusion examples are listed here.

Among the above track-to-track fusion methods, the Bar-Shalom-Campo algorithm is simple and easy to implement, less sensitive to measurement errors, and has better fusion performance for radars with a great difference in detection accuracy. Considering the characteristics of target detection with a T/R-R composite compact HFSWR system, the fuzzy double-threshold association method, and the Bar-Shalom-Campo algorithm are, respectively, selected for track-to-track association and fusion in this article.

Unlike noncoherent marine radar [43], HFSWR can also provide target Doppler velocity in addition to position. As vessels usually move at relatively low speeds, longer coherent integration time (CIT) is usually required for maritime target detection so that accurate Doppler velocity can be achieved. As shown in Fig. 1, the radial velocity V_R, and the elliptical velocity V_E can be measured by the T/R monostatic radar and T-R bistatic radar, respectively. For a specific target with a known position, once the two Doppler velocities V_R and V_E are obtained at a sampling instant, they can be combined to estimate the vector velocity.

Under a T/R-R configuration, since the target positions associated with V_R and V_E for a specific time may not refer to a same location, the two Doppler velocities can only be used to calculate the vector velocity after track fusion. The remainder of this article is organized as follows. The target plot and track representations with a T/R-R composite compact HFSWR are provided in Section II. The proposed method is described in detail in Section III. In Section IV, experimental results are presented and analyzed. Theoretical and experimental analysis of the estimation error is provided in Section V and conclusion are drawn in Section VI.

II. Target Plot and Track Representations for T/R-R Composite Compact HFSWR

HFSWR depicts a target with three kinematic parameters, range, bearing, and Doppler velocity. The range and bearing determine a target's position, while Doppler velocity is the radial component of the target's true speed. The T/R-R composite radar system is designed for sea-surface target detection in a 2D plane with due North and due East as the positive directions of the vertical and horizontal axes, respectively. As shown in Fig. 1, the T/R and R radar stations denoted with red solid triangles are located at $(lon_{T/R}, lat_{T/R})$ and (lon_R, lat_R), respectively. φ_L denotes the intersection angle between the baseline and East direction. The target is located at $S(lon_S, lat_S)$. Two linear phased receiving antenna arrays consisting of a few equally spaced antenna elements, which are labeled as receiving array 1 at the T/R station and receiving array 2 at the R station, are denoted using black lines with green and red dots indicating

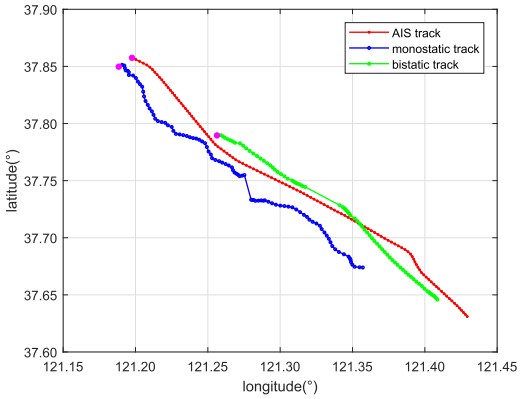

Fig. 2. Tracking results of a target with a T/R monostatic radar and a T-R bistatic radar.

the antenna elements. Once the receiving antenna arrays are deployed, their boresights are determined as φ_T and φ_R referenced with respect to the due North, respectively. Under the T/R-R configuration, one target has two sets of representations. The T/R monostatic radar represents a target with a state vector $[r_T\ \theta_T\ V_R]^T$, where r_T denotes the distance between a target and T/R radar site, θ_T represents the target bearing with respect to the due North, V_R is the target radial velocity. While the T-R bistatic radar represents it with a state vector $[r_R\,\theta_R\,V_E]^T$, where r_R denotes the distance between a target and the receiver of a T-R radar, θ_R represents the target bearing, V_E is the target elliptical velocity along the direction of the bistatic bisection. For both T/R monostatic and T-R bistatic radars, target plot data can be collected at every sampling instant, and plot data sequences can be obtained after several consecutive sampling instants, with each plot represented by a corresponding state vector. Then a multitarget tracking algorithm can be applied to these plot data sequences to obtain two target track sets, represented as $T_1 = \{track_i^1 | i = 1, 2, \ldots, m\}$ and $T_2 = \{track_i^2 | i = 1, 2, \ldots, n\}$, respectively, where m, n are the numbers of monostatic and bistatic tracks.

Fig. 2 illustrates the tracking results of a specific target obtained by a T/R monostatic radar and a T-R bistatic radar using converted measurement Kalman filter (CMKF) [44], the corresponding automatic identification system (AIS) track is also shown for comparison, and the mauve solid dots indicate the starting points of tracks. As shown in Fig. 2, the tracks obtained by two radars behave differently in positions due to different measurement errors.

III. Proposed Method

The proposed vessel vector velocity estimation method consists of a track association and fusion module, and a vector velocity estimation module. First, the track association and fusion module are applied to the track sets T_1 and T_2 to determine the track pairs belonging to the same target and merge them to produce estimated tracks with higher positioning accuracy. Then the vector velocity estimation module is used to estimate the vector velocity based on each fused position, radial velocity measured by the T/R radar, and elliptical velocity measured by the T-R radar. These two modules will be described in detail in the following sections.

A. Track Association and Fusion

The goal of track association and fusion is to exploit the complementary information of target measurements simultaneously obtained by T/R monostatic radar and T-R bistatic radar to improve target positioning accuracy. First, the fuzzy double-threshold track-to-track association method is applied to the two track sets T_1 and T_2 to determine the associated track pairs. Then, for a specific track pair, the track-to-track fusion method based on Bar-Shalom-Campo is used to produce a fused track. As the converted measurement Kalman filter is implemented under Cartesian coordinate, to clearly describe the track-to-track association and fusion procedure, the state of a target detected by T/R monostatic radar at sampling time k in Cartesian coordinate system is denoted as $\boldsymbol{s}_1(k) = [x_k^1\ \dot{x}_k^1\ y_k^1\ \dot{y}_k^1]^T$, where x_k^1, y_k^1 are the target's locations in x–y coordinate, $\dot{x}_k^1$ and $\dot{y}_k^1$ denote the target's velocities in x and y directions. During the tracking process, the state estimation error covariance matrix can be obtained and denoted as $\boldsymbol{P}_1(k)$. Similarly, the corresponding representations for T-R bistatic radar are denoted as $\boldsymbol{s}_2(k) = [x_k^2\ \dot{x}_k^2\ y_k^2\ \dot{y}_k^2]^T$, $\boldsymbol{P}_2(k)$, respectively. The subscript k is omitted in the flowing descriptions for simplicity. Based on the above representations, the estimated target state at sampling time k after track-to-track fusion can be expressed as

$$\boldsymbol{s} = \boldsymbol{P}_2(\boldsymbol{P}_1 + \boldsymbol{P}_2)^{-1}\boldsymbol{s}_1 + \boldsymbol{P}_1(\boldsymbol{P}_1 + \boldsymbol{P}_2)^{-1}\boldsymbol{s}_2 \tag{1}$$

and the corresponding state estimation error covariance matrix is

$$\boldsymbol{P} = \boldsymbol{P}_1(\boldsymbol{P}_1 + \boldsymbol{P}_2)^{-1}\boldsymbol{P}_2. \tag{2}$$

However, it is worth noting that the T/R monostatic and T-R bistatic radars share the same transmitting antenna, have similar receiving antenna arrays, and operate simultaneously under the same detection environment. Thus, they have similar priori estimation error or process noise so that the error correlation between their local estimates should be considered during the track-to-track fusion procedure. The state estimation difference of an associated track pair is expressed as

$$D_{12} = \boldsymbol{s}_1 - \boldsymbol{s}_2 \tag{3}$$

and its covariance matrix is

$$E[D_{12}{D_{12}}^T] = \boldsymbol{P}_1 + \boldsymbol{P}_2 - \boldsymbol{P}_{12} - \boldsymbol{P}_{21} \tag{4}$$

where $\boldsymbol{P}_{12}$ and $\boldsymbol{P}_{21}$ are estimation error cross covariance matrices which can be calculated as

$$\begin{aligned}\boldsymbol{P}_{12}(k) &= (\boldsymbol{I} - \boldsymbol{K}\boldsymbol{H})(\boldsymbol{\Phi}\boldsymbol{P}_{12}(k-1)\boldsymbol{\Phi}^T + \boldsymbol{Q})(\boldsymbol{I} - \boldsymbol{K}\boldsymbol{H})^T \\ \boldsymbol{P}_{21}(k) &= (\boldsymbol{I} - \boldsymbol{K}\boldsymbol{H})(\boldsymbol{\Phi}\boldsymbol{P}_{21}(k-1)\boldsymbol{\Phi}^T + \boldsymbol{Q})(\boldsymbol{I} - \boldsymbol{K}\boldsymbol{H})^T\end{aligned} \tag{5}$$

where $\boldsymbol{I}$, $\boldsymbol{K}$, $\boldsymbol{\Phi}$, $\boldsymbol{H}$, and $\boldsymbol{Q}$ are the identity matrix, Kalman gain, state transition matrix, measurement matrix, and process noise covariance matrix, respectively, which can be obtained during Kalman filtering procedure.

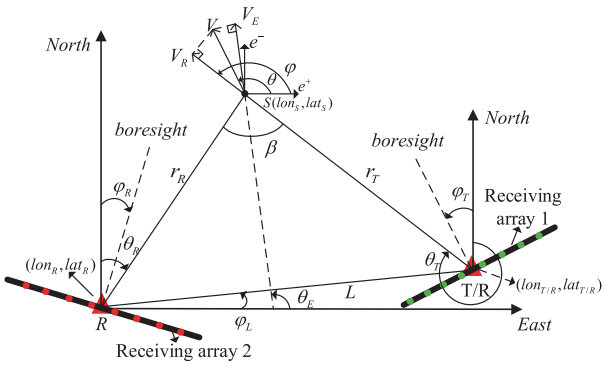

Fig. 3. Schematic diagram of vector velocity estimation.

Based on the above analysis, the final fused state and the corresponding state estimation error covariance matrix can be written as

$$\begin{aligned}\bar{\boldsymbol{s}} &= \boldsymbol{s}_1 + (\boldsymbol{P}_1 - \boldsymbol{P}_{12})(\boldsymbol{P}_1 + \boldsymbol{P}_2 - \boldsymbol{P}_{12} - \boldsymbol{P}_{21})^{-1}(\boldsymbol{s}_2 - \boldsymbol{s}_1)\\ \boldsymbol{P} &= \boldsymbol{P}_1 - (\boldsymbol{P}_1 - \boldsymbol{P}_{12})(\boldsymbol{P}_1 + \boldsymbol{P}_2 - \boldsymbol{P}_{12} - \boldsymbol{P}_{21})^{-1}\\ &\quad \times (\boldsymbol{P}_1 - \boldsymbol{P}_{21}).\end{aligned} \tag{6}$$

B. Vessel Vector Velocity Estimation Method

The schematic diagram of vessel vector velocity estimation with T/R-R composite compact HFSWR is shown in Fig. 3. Suppose a target moves at a velocity $\boldsymbol{V}$ with V as its amplitude and θ as its heading referenced with the due East, its position at current moment is S. With two radar sites separated by a known distance L, the bistatic angle β is formed. As mentioned in Section II, the T/R monostatic radar represents the target with a state vector $[r_T\ \theta_T\ V_R]^T$, while the T-R bistatic radar represents it with a state vector $[r_R\ \theta_R\ V_E]^T$. Actually, the T-R bistatic radar directly measures the total distance $\rho = r_T + r_R$ that is the transmitter-target-receiver distance, the range r_R between the target and receiving site can be calculated via the triangle relation. φ and θ_E denote the intersection angles between the directions of radial velocity V_R, elliptical velocity V_E, respectively, and baseline L.

As a Doppler radar, the Doppler velocity V_R measured by T/R monostatic radar is along the radar looking direction, while the isorange contour of a T-R bistatic radar forms an ellipse whose two foci are, respectively, at the locations of the transmitter and receiver, the Doppler velocity V_E is along the bisector of the bistatic angle, which is perpendicular to the tangent direction of the ellipse.

With the locations of two radar sites being known, the bistatic angle β can be calculated in two ways for each plot in a fused track. First, it can be calculated according to the triangle relationship as

$$\begin{aligned}\beta &= \arccos\left(\frac{{r_R}^2 + {r_T}^2 - L^2}{2 r_T r_R}\right)\\ r_R &= \frac{\rho^2 - L^2}{2[\rho - L\sin(\theta_R + \varphi_L)]}.\end{aligned} \tag{7}$$

Second, it can also be calculated using the targets' bearings θ_T and θ_R as

$$\beta = \begin{cases}\theta_R - \theta_T, & \theta_R \geq \theta_T\\ 2\pi + \theta_R - \theta_T, & \theta_R < \theta_T.\end{cases} \tag{8}$$

Denoting $\boldsymbol{e}^+$ and $\boldsymbol{e}^-$ as the unit vectors of two orthogonal axes with $\boldsymbol{e}^-$ along the due North as shown in Fig. 3, then the vector velocity $\boldsymbol{V}$ can be expressed as

$$\boldsymbol{V} = V\cos\theta \boldsymbol{e}^+ + V\sin\theta \boldsymbol{e}^-. \tag{9}$$

According to the projection relationship, the radial velocity V_R and elliptical velocity V_E can be derived as

$$\begin{aligned}V_R &= V\cos(\theta - \varphi)\\ V_E &= V\cos(\theta - \theta_E)\cos\left(\frac{\beta}{2}\right)\end{aligned} \tag{10}$$

where

$$\begin{aligned}\varphi &= \begin{cases}\frac{\pi}{2} - \theta_T, & \theta_T \in (0, \frac{\pi}{2}]\\ \frac{5\pi}{2} - \theta_T, & others\end{cases}\\ \theta_E &= \varphi - \frac{\beta}{2}.\end{aligned} \tag{11}$$

From (9)–(11), the velocity amplitude V can be derived as

$$V = \sqrt{\frac{4\left[{V_E}^2 + {V_R}^2\cos^2(\frac{\beta}{2}) - 2V_E V_R\cos^2(\frac{\beta}{2})\right]}{\sin^2\beta}}. \tag{12}$$

It can be drawn from (12) that the velocity amplitude is determined in terms of radial velocity V_R, elliptical velocity V_E, and bistatic angle β.

The direction of the velocity (i.e., θ in Fig. 3) is derived as

$$\theta = \arctan\left(\frac{V_E\cos\varphi - V_R\cos(\frac{\beta}{2})\cos\theta_E}{V_R\cos(\frac{\beta}{2})\sin\theta_E - V_E\sin\varphi}\right). \tag{13}$$

Then the vessel heading which is referenced with respect to the due North can be obtained as

$$heading = \begin{cases}\frac{\pi}{2} - \theta, & \theta \in [0, \frac{\pi}{2}]\\ \frac{5\pi}{2} - \theta, & others.\end{cases} \tag{14}$$

It should be noted that φ_L only affects the calculation of r_R in (7). If (8) is used to calculate the bistatic angle β, φ_L does not need to be considered.

As both the radial velocity V_R and elliptical velocity V_E are the projected components of a target's vector velocity, it should be pointed out that the parallelogram rule for vector composition is not applicable here except for the case when the direction of radial velocity is perpendicular to that of the elliptical velocity. The proposed vessel vector velocity estimation method is summarized in Algorithm 1, and the flowchart is shown in Fig. 4.

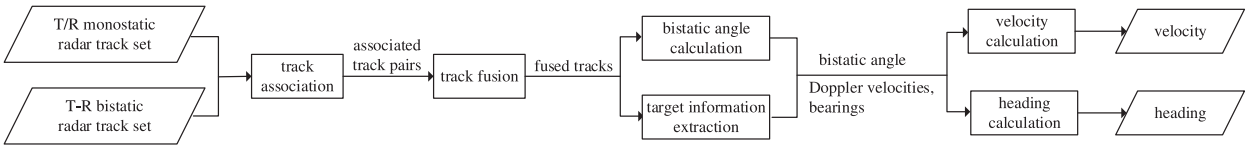

Fig. 4. Flowchart of vector velocity estimation.

Algorithm 1: Vessel Vector Velocity Estimation Method.

Input: Track sets T_1 and T_2 obtained from T/R monostatic and T-R bistatic radars data.

Output: The speed and heading results sequences.

1: The track-to-track association method based on fuzzy double-threshold is applied to the track sets T_1 and T_2 to produce associated track pairs.

2: The associated track pairs are merged to produce N fused tracks by track-to-track fusion method based on Bar-Shalom-Campo algorithm.

3: For each fused track out of N tracks

For each plot of a fused track with M plots

i. The bistatic angle β is calculated by (7) or (8).

ii. Equation (12) is used to calculate the magnitude of velocity with measured radial velocity V_R, elliptical velocity V_E, and calculated bistatic angle β.

iii. Equations (13) and (14) are used to calculate the target heading that is equivalent to the direction of target velocity.

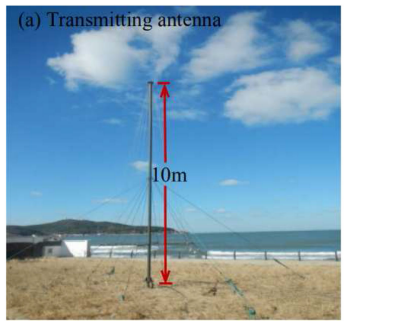

(a)

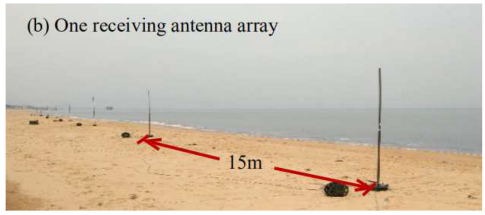

(b)

Fig. 5. Transmitting antenna and one receiving antenna array of the developed T/R-R composite compact HFSWR system.

IV. Experiments and Discussions

A. System and Data Description

In order to demonstrate the effectiveness of the proposed method, vector velocity estimation tests were conducted using the field data recorded by a newly developed T/R-R composite compact HFSWR system operated at the North China Sea on April 30, 2019. The radar system consists of one transmitter, one transmitting antenna, one receiver, two similar receiving antenna arrays, and one display and control system. Its geometric configuration is shown in Fig. 1 with φ_L being 10.35°. The photos of its transmitting antenna and one receiving antenna array are shown in Fig. 5. The key parameters for the radar system is listed in Table I. The synchronization of two separately deployed radars was realized using a GPS time reference. Synchronous AIS data were used as ground truth for comparisons and evaluations.

TABLE I
Parameters for the T/R-R Composite Compact HFSWR

Parameter	Specification
Location of T/R radar	Weihai(122.07°E, 37.54°N)
Location of T-R receiver	Yantai (121.49°E, 37.45°N)
Baseline distance L	52 km
φ_L	10.35°
Waveform	FMICW
Frequency	4.7 MHz
Transmit antenna	Omnidirectional log-periodic antenna
Receive antenna	8 active whip antenna units
Inter-element distance	15 m
Maximum peak power	480 W
Maximum detection range	100 km
Coherent integration time	262.144 s
Data rate	1 frame/min

B. Track Results

The target tracking method combining converted measurement Kalman filter and data association based on minimal cost [11], [12] was applied to the plot data sequences simultaneously collected by the T/R monostatic radar and T-R bistatic radar, respectively, to produce two corresponding track sets. Then track-to-track association method based on fuzzy double-threshold and track-to-track fusion method based on Bar-Shalom-Campo algorithm were sequentially applied to get the associated track pairs and fused tracks. Two vessel examples, named target 1 and target 2 with reported information by AIS listed in Table II, were selected for analysis. The monostatic radar tracks, bistatic radar tracks, fused tracks, and corresponding AIS tracks are shown in Fig. 6, where the mauve solid dots indicate the starting points of tracks.

C. Vector Velocity Estimation Results

1) Results of an Intuitive Method: The intuitive method for speed estimation is to divide the distance by the time interval

TABLE II
GENERAL INFORMATION FOR TWO EXAMPLE TARGETS

	Target 1	Target 2
Ship Name	HUI RONG	HENGYU 2
MMSI	413331140	413500170
Ship Type	Cargo	Cargo
Length (m)	98	98
Width (m)	16	16

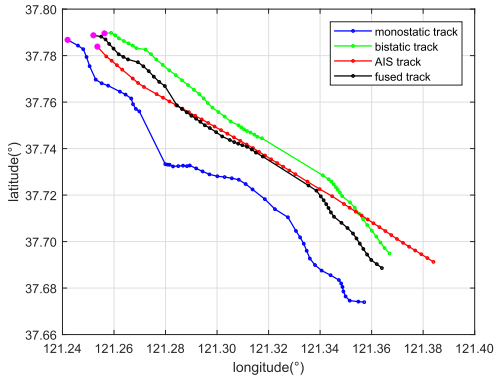

(a)

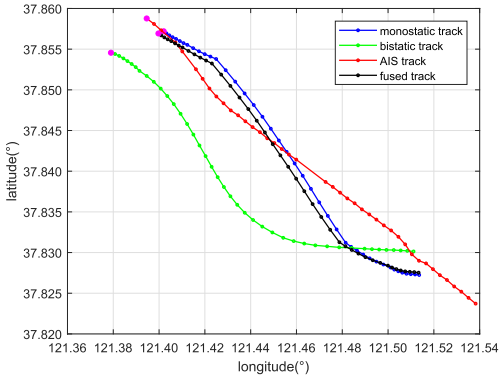

(b)

Fig. 6. Track comparisons among monostatic radar tracks, bistatic radar tracks, fused tracks, and matched AIS tracks. (a) Track comparisons for target 1. (b) Track comparisons for target 2.

between two adjacent plots, while that for heading estimation is to determine the direction of two consecutive target positions. First, the intuitive target speed and heading estimation method are applied to the position data sequences obtained from the monostatic and fused radar tracks for target 1, respectively, and the obtained results together with the corresponding AIS data are shown in Fig. 7. It can be observed from the AIS data that target 1 moves at nearly constant speeds and headings. However, the estimated speed and heading data sequences from both the monostatic radar track and fused radar track present significant fluctuations and large deviations from their true values. The root-mean-square-errors (rmse) of the estimated speed data sequences from monostatic radar track and fused radar track are 36.27 and 21.34 km/h, respectively, while those for the estimated heading data sequences are 23.52° and 15.33°, respectively. Although the estimation accuracy of speed and heading has been improved for the fused radar track, the results

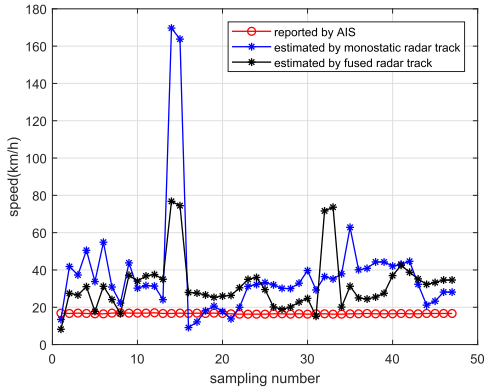

(a)

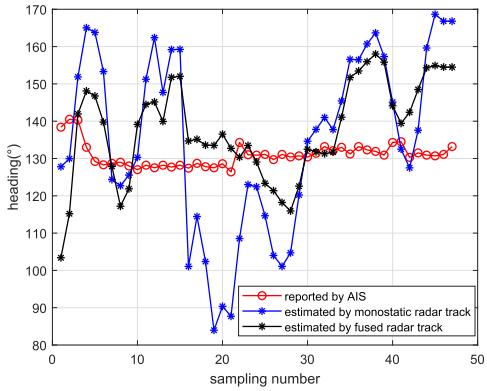

(b)

Fig. 7. Estimated results of speed and heading for target 1 using an intuitive method. (a) Speed estimation results. (b) Heading estimation results.

are still far from satisfactory. Therefore, the intuitive method fails to provide accurate speed and heading estimations from the compact HFSWR data. Next, the proposed velocity estimation method will be tested.

2) Results of the Proposed Method: Since the proposed vector velocity estimation method depends on target bistatic angle or bearing and Doppler velocity, these parameters for the aforementioned two example targets will be analyzed first. The matched AIS data, which provide ground-truth information including target positions in longitudes and latitudes, true speeds, headings, etc., were used to evaluate the accuracy of these measured parameters. First, these kinematic parameters of AIS were converted according to corresponding radar coordinates. Given the locations of Weihai and Yantai radar sites, target range and bearing data sequences can be generated using target positions in longitudes and latitudes. The radial velocity and the elliptical velocity data sequences can be obtained by projecting target velocities onto the radial directions of the T/R monostatic radar and the directions of bistatic bisection of the T-R bistatic radar according to (10).

The target bearings θ_T and θ_R measured by the T/R monostatic radar and T-R bistatic radar along with their corresponding AIS data for two example targets are shown in Fig. 8. It can be observed that the variation trends of bearings have a good agreement with those of their true values with rmses of 1.40°, 1.28°, 0.81°, and 4.27°, respectively. The results show that the

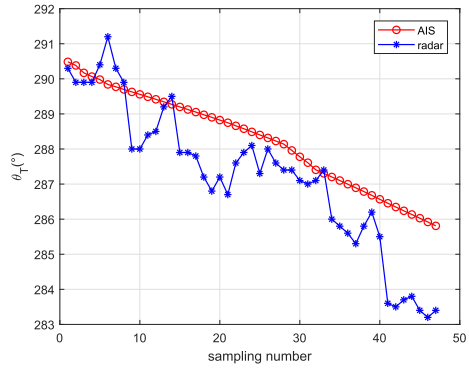

(a)

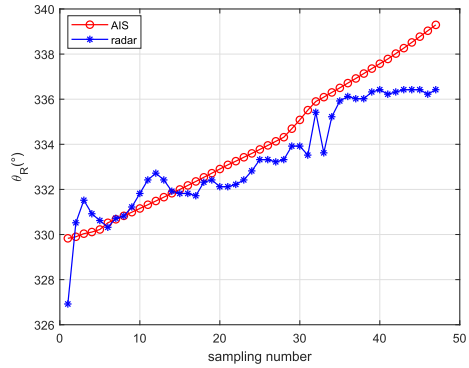

(b)

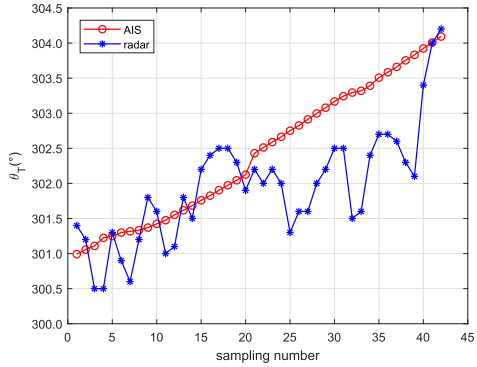

(c)

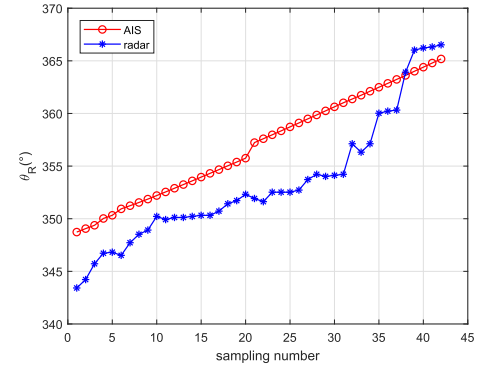

(d)

Fig. 8. Bearing data sequences of target 1 and target 2. (a) Bearing data sequence of target 1 obtained by T/R radar. (b) Bearing data sequence of target 1 obtained by T-R radar. (c) Bearing data sequence of target 2 obtained by T/R radar. (d) Bearing data sequence of target 2 obtained by T-R radar.

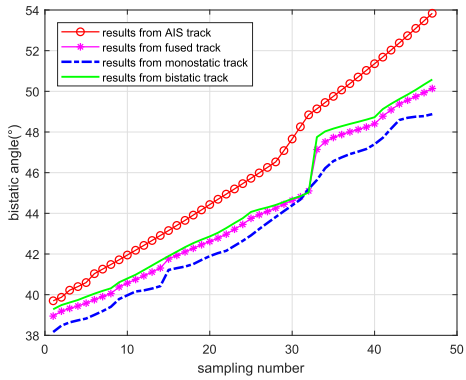

(a)

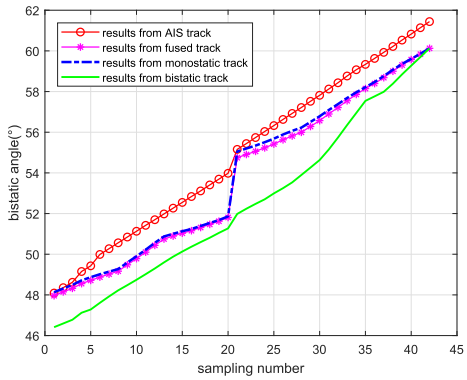

(b)

Fig. 9. Comparisons of bistatic angle data sequences. (a) Bistatic angle data sequence comparison for target 1. (b) Bistatic angle data sequence comparison for target 2.

developed compact system can provide target bearings with acceptable accuracy.

Then the bistatic angle data sequences calculated according to (8) from the bearing data in the monostatic radar tracks, bistatic radar tracks, fused tracks, as well as the corresponding AIS tracks for two example targets are shown in Fig. 9. It is illustrated that the bistatic angles of both targets gradually increase since both of them move toward the baseline. The ranges of bistatic angle are from 40° to 54°, and from 48° to 61° for target 1 and target 2, respectively. There are obvious deviations between bistatic angle data sequences calculated from the fused radar tracks and ground-truth AIS tracks with RMSEs of 2.22° and 1.24° for target 1 and target 2, respectively. The errors in the bistatic angle calculation are due to the low spatial resolution and may deteriorate the vector velocity estimation performance. It should also be noticed that the bistatic angle data sequences calculated from the monostatic and bistatic radar tracks of target 1 and target 2 deviate from their true values in different ways due to different positioning errors. For target 1, the bistatic angle data sequence calculated from the bistatic radar track is closer to its true value than that obtained from the monostatic radar track, but the opposite is true for target 2. Fortunately, good results can always be guaranteed for the bistatic angle data sequences calculated from the fused radar tracks. The abrupt changes appearing around the 32nd data point in Fig. 9(a) and

the 20th data point in Fig. 9(b) in the fused radar track are due to the position differences caused by missed target detections.

Next, the radial velocity data sequences measured by the T/R monostatic radar, elliptical velocity data sequences measured by the T-R bistatic radar, and the counterparts calculated by AIS data for two example targets are shown in Fig. 10. As is shown in Fig. 10, the variation trends of the Doppler velocity data sequences obtained from radar and AIS agree well with each other with RMSEs of 0.48, 0.40, 0.48, 0.85 km/h, respectively. The results verify that the developed radar system achieves a higher Doppler resolution.

The proposed vector velocity estimation method was applied to the data of the fused radar tracks and the obtained results are shown in Fig. 11, the corresponding AIS data are also shown for comparison. It is observed that the variation trends of the estimated speed and heading data sequences agree well with those of their ground truth. It is noticed in Fig. 11(c) that the 34th speed data point of target 2 shows a large bias, this is due to the large deviation of its measured elliptical velocity by T-R bistatic radar from its true value [see Fig. 10(d)]. Then the speed and heading errors between the estimated values and AIS data were calculated for two example targets, and the error distributions are illustrated in Fig. 12. Statistical analysis shows that majority of speed errors is less than 0.7 km/h, while majority of heading errors is less than 7°. The RMSEs of speed are 0.55 and 0.41 km/h for target 1 and target 2, respectively, while the corresponding RMSEs of heading are 2.39° and 5.46°, respectively. The average RMSEs of speed and heading are 0.48 km/h and 3.9°. These results are much better than those of the intuitive method.

The measurement errors of bistatic angle and Doppler velocity will influence the vector velocity estimation accuracy. If the speed and heading data sequences of target 1 and target 2 were estimated using the bistatic angles β calculated from their fused radar tracks, but radial velocities V_R and elliptical velocities V_E calculated from their matched AIS tracks. The obtained results are shown in Fig. 13. It is observed that the speed and heading estimation accuracy has been considerably improved with RMSEs of 0.06 km/h, 0.85° and 0.12 km/h, 1.6° for target 1 and target 2, respectively. However, if the bistatic angles β are calculated using the data from their matched AIS tracks, and radial velocities V_R and elliptical velocities V_E are calculated from their fused radar tracks, the obtained estimations are similar to those shown in Fig. 11 with RMSEs of 0.43 km/h, 2.04° for target 1 and 0.45 km/h, 5.14° for target 2, which indicates that the measurement error of Doppler velocity has stronger influence on the vector velocity estimation.

Once a target's speed and heading data sequences are obtained, its vector velocity data sequence is achieved. The vector velocities for part of plots from target 1 are shown in Fig. 14, with the red plots representing the target positions provided by its AIS track and black arrows indicating the velocity magnitude and direction calculated using the Doppler velocities measured by the radar system and bistatic angles estimated from the fused radar tracks. Fig. 14 illustrates that the estimated heading is consistent with the tangent direction of the target trajectory. Taking the first plot of the fused radar track as the starting point, a new track can be regenerated with newly predicted plots using

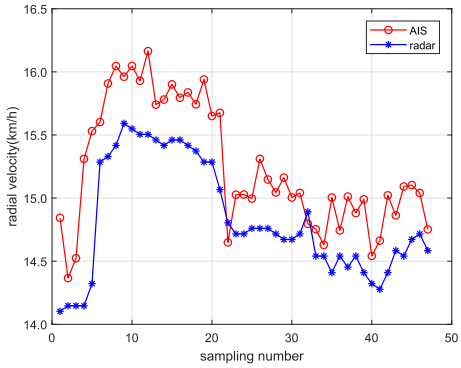

(a)

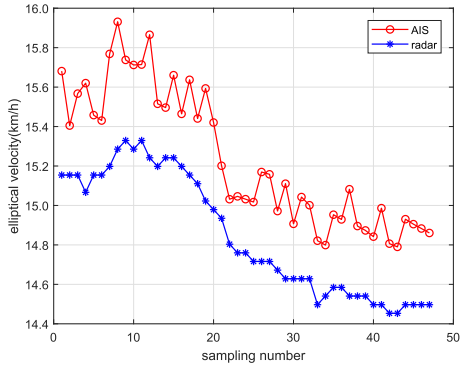

(b)

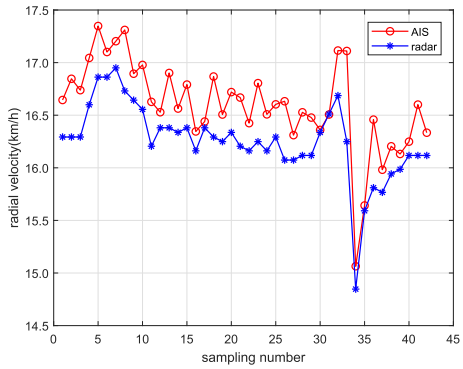

(c)

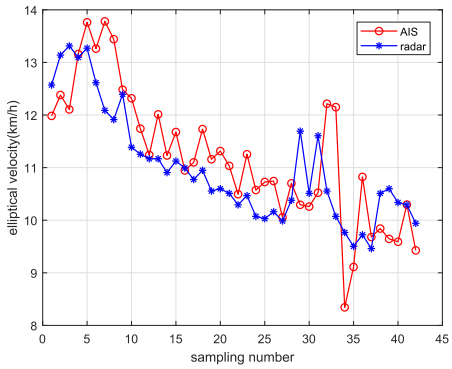

(d)

Fig. 10. Doppler velocity comparisons between radar and AIS. (a) Radial velocity comparison for target 1. (b) Elliptical velocity comparison for target 1. (c) Radial velocity comparison for target 2. (d) Elliptical velocity comparison for target 2.

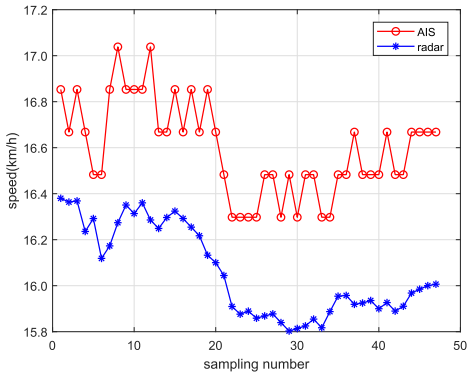

(a)

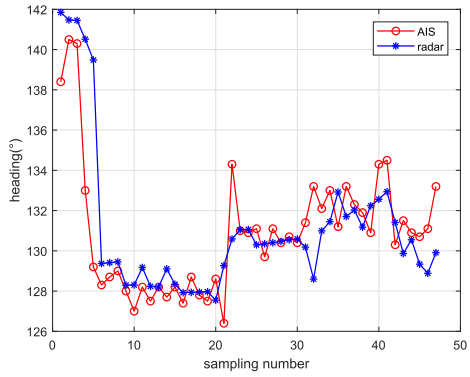

(b)

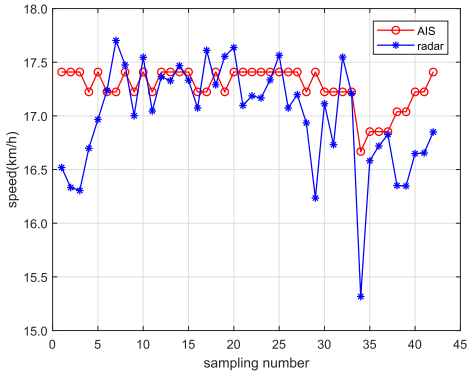

(c)

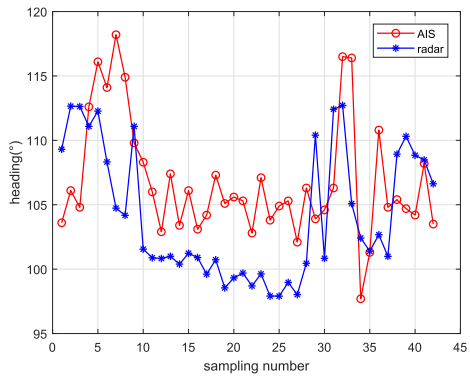

(d)

Fig. 11. Estimated results of speed and heading using field radar data. (a) Speed of target 1. (b) Heading of target 1. (c) Speed of target 2. (d) Heading of target 2.

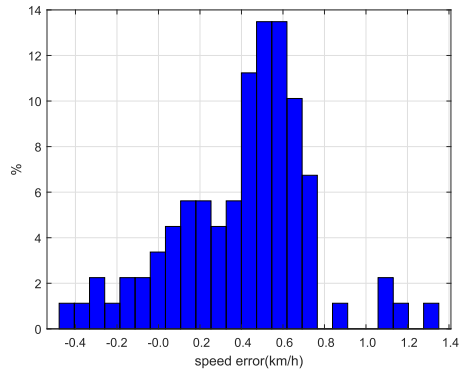

(a)

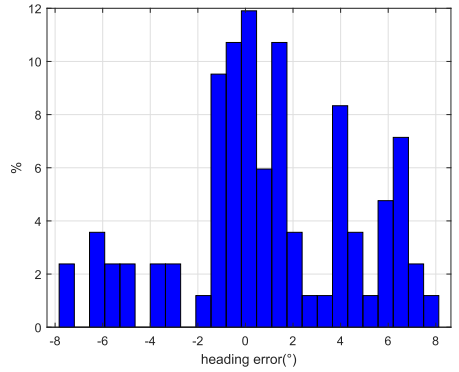

(b)

Fig. 12. Error distributions of speed and heading. (a) Error distribution of speed. (b) Error distribution of heading.

the estimated vector velocity. The retracking results of target 1 and target 2 are shown in Fig. 15, which illustrates that the newly generated tracks are smoother than the original fused tracks and have better consistency with those of the corresponding AIS tracks. The deviations between the retracked results and corresponding AIS tracks are mainly due to the positioning error of the first plot of the fused radar tracks.

V. Estimation Error Analysis

Limited by the spatial and Doppler resolutions of compact HFSWR, the radial velocity V_R, elliptical velocity V_E, bearings θ_T and θ_R cannot be accurately measured, thus affecting the target vector velocity estimated by the proposed method. To analyze the influence of measurement errors of Doppler velocity and bistatic angle on vector velocity estimation accuracy, the expressions of estimation error for speed and heading are theoretically derived and verified by simulations.

A. Estimation Error Derivation

Substituting the bistatic angle β with the expressions in (8) and (12) can be rewritten as

$$V = \sqrt{\frac{4\left[{V_E}^2 + {V_R}^2\cos^2\left(\frac{\theta_R-\theta_T}{2}\right) - 2V_E V_R \cos^2\left(\frac{\theta_R-\theta_T}{2}\right)\right]}{\sin^2(\theta_R-\theta_T)}}. \tag{15}$$

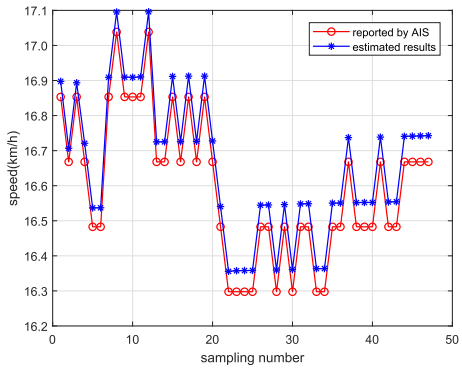

(a)

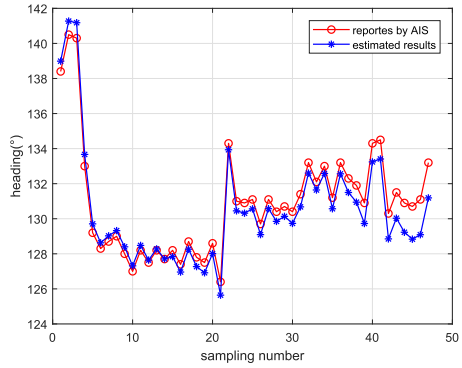

(b)

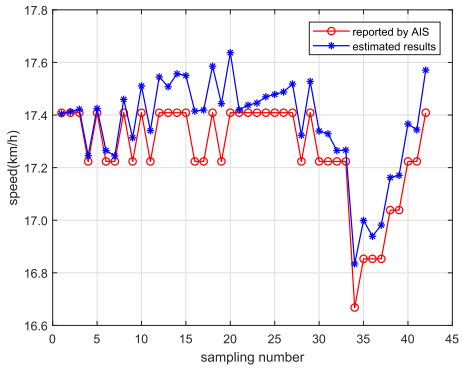

(c)

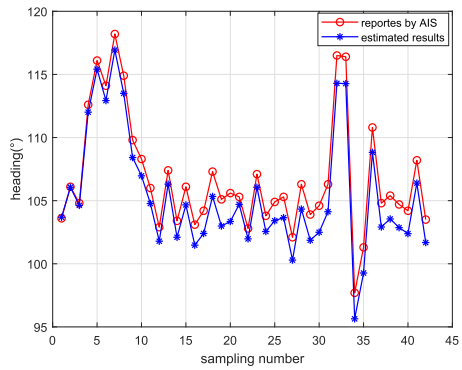

(d)

Fig. 13. Speed and heading estimation results with accurate Doppler velocities and measured bistatic angles. (a) Speed comparison for target 1. (b) Heading comparison for target 1. (c) Speed comparison for target 2. (d) Heading comparison for target 2.

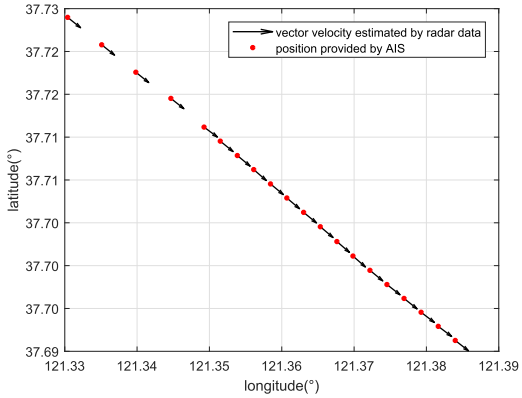

Fig. 14. Illustration of the estimated vector velocities for target 1.

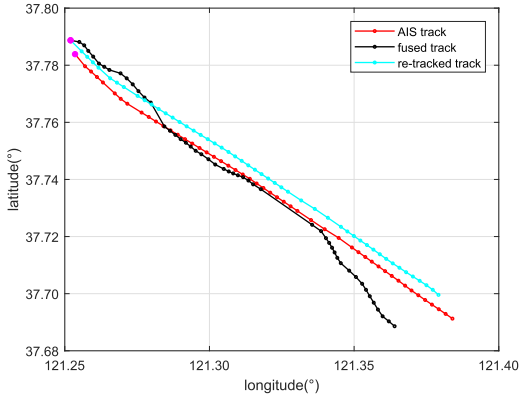

(a)

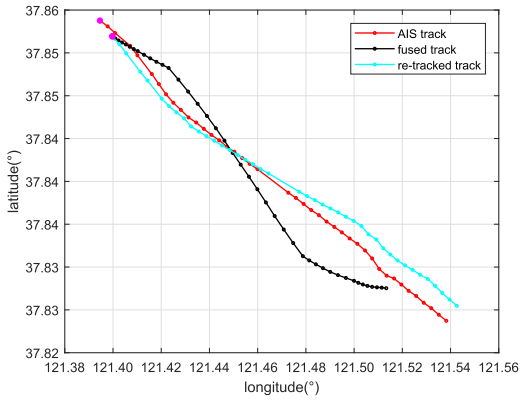

(b)

Fig. 15. Track comparison between fused tracks and regenerated tracks. (a) Fused and regenerated tracks of target 1. (b) Fused and regenerated tracks of target 2.

Full differential operators are applied to both sides of (15) to get dV as

$$dV = \frac{\partial V}{\partial V_E} dV_E + \frac{\partial V}{\partial V_R} dV_R + \frac{\partial V}{\partial \theta_T} d\theta_T + \frac{\partial V}{\partial \theta_R} d\theta_R \quad (16)$$

where dV_R and dV_E represent the measurement errors of the radial and elliptical velocities, respectively, which rely on the Doppler resolution of the radar system. $d\theta_R$ and $d\theta_T$ denote the measurement errors of target bearings, which are determined by

the aperture size of the receiving antenna array. $\frac{\partial V}{\partial V_E}$, $\frac{\partial V}{\partial V_R}$, $\frac{\partial V}{\partial \theta_T}$, $\frac{\partial V}{\partial \theta_R}$ denote the error transfer coefficients of the four kinematic parameters and are expressed as

$$\begin{aligned}
\frac{\partial V}{\partial V_E} &= \frac{4[V_E - V_R\cos^2(\frac{\theta_R-\theta_T}{2})]}{V\sin^2(\theta_R-\theta_T)} \\
\frac{\partial V}{\partial V_R} &= \frac{4(V_R - V_E)\cos^2(\frac{\theta_R-\theta_T}{2})}{V\sin^2(\theta_R-\theta_T)} \\
\frac{\partial V}{\partial \theta_T} &= \frac{V_R^2 + V^2\cos(\theta_R-\theta_T) - 2V_EV_R}{V\sin(\theta_R-\theta_T)} \\
\frac{\partial V}{\partial \theta_R} &= -\frac{V_R^2 + V^2\cos(\theta_R-\theta_T) - 2V_EV_R}{V\sin(\theta_R-\theta_T)}.
\end{aligned} \tag{17}$$

It can be found that $\frac{\partial V}{\partial \theta_T} = -\frac{\partial V}{\partial \theta_R}$. Similarly, (13) can be rewritten as

$$\theta = \arctan\left(\frac{V_E\sin\theta_T - V_R\cos(\frac{\theta_R-\theta_T}{2})\sin(\frac{\theta_R+\theta_T}{2})}{V_R\cos(\frac{\theta_R-\theta_T}{2})\cos(\frac{\theta_R+\theta_T}{2}) - V_E\cos\theta_T}\right). \tag{18}$$

Applying full differential operators on both sides of (18) gives $d\theta$ as

$$d\theta = \frac{\partial\theta}{\partial V_E}dV_E + \frac{\partial\theta}{\partial V_R}dV_R + \frac{\partial\theta}{\partial\theta_T}d\theta_T + \frac{\partial\theta}{\partial\theta_R}d\theta_R \tag{19}$$

where the corresponding error transfer coefficients are expressed as

$$\begin{aligned}
\frac{\partial\theta}{\partial V_E} &= -\frac{V_R\sin(\theta_R-\theta_T)}{2[V_E^2 + V_R^2\cos^2(\frac{\theta_R-\theta_T}{2}) - 2V_EV_R\cos^2(\frac{\theta_R-\theta_T}{2})]} \\
\frac{\partial\theta}{\partial V_R} &= \frac{V_E\sin(\theta_R-\theta_T)}{2[V_E^2 + V_R^2\cos^2(\frac{\theta_R-\theta_T}{2}) - 2V_EV_R\cos^2(\frac{\theta_R-\theta_T}{2})]} \\
\frac{\partial\theta}{\partial\theta_T} &= \frac{V_EV_R + 2V_EV_R\cos^2(\frac{\theta_R-\theta_T}{2}) - 2V_E^2 - V_R^2\cos^2(\frac{\theta_R-\theta_T}{2})}{2[V_E^2 + V_R^2\cos^2(\frac{\theta_R-\theta_T}{2}) - 2V_EV_R\cos^2(\frac{\theta_R-\theta_T}{2})]} \\
\frac{\partial\theta}{\partial\theta_R} &= \frac{V_EV_R\cos(\theta_R-\theta_T) - V_R^2\cos^2(\frac{\theta_R-\theta_T}{2})}{2[V_E^2 + V_R^2\cos^2(\frac{\theta_R-\theta_T}{2}) - 2V_EV_R\cos^2(\frac{\theta_R-\theta_T}{2})]}.
\end{aligned} \tag{20}$$

Equations (16) and (19) indicate that the estimation error of speed and heading depends on the measurement errors of radial velocity V_R, elliptical velocity V_E, bearings θ_T and θ_R, as well as the error transfer coefficients depicted in (17) and (20). To provide a more general estimation error evaluation of the proposed vector velocity estimation method, the following two experiments were designed to analyze the estimation errors.

B. Effect of Bistatic Angle on Estimation Errors

Compact HFSWR provides relatively accurate Doppler velocity but low-resolution bearing, and bistatic angles are determined by target positions or bearings, the variation trends of speed and heading estimation errors with varying bistatic angles will be analyzed first with fixed Doppler velocities.

It is noticed that the radial velocity V_R and elliptical velocity V_E are two projected components of target true speed, thus they correlate with each other. A typical Doppler velocity pair with $V_R = 14.84$ km/h, $V_E = 15.68$ km/h was set and kept unchanged in the experiment. According to the statistical analysis

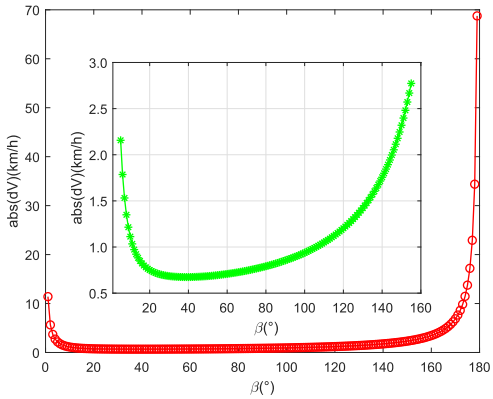

(a)

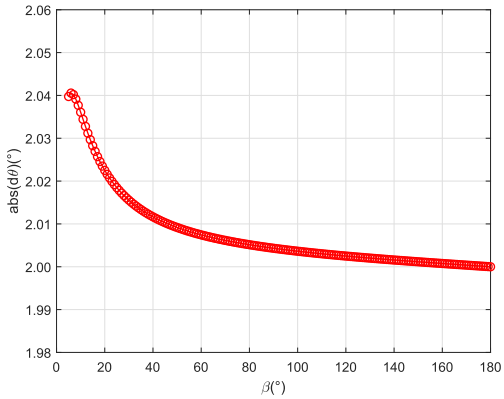

(b)

Fig. 16. Absolute estimation error of speed and heading. (a) Absolute estimation error of speed. (b) Absolute estimation error of heading.

of the measurement error of the developed HFSWR system, the measurement errors of Doppler velocity and bearing were set as follows:

$$dV_E = 0.6 \text{ km/h}, dV_R = 0.5 \text{ km/h}, d\theta_T = d\theta_R = 2^\circ.$$

Since similar linear phased antenna arrays were employed as receiving antennas [15] for both T/R monostatic radar and T-R bistatic radar, and the digital beam forming method [3] was used to estimate target bearings θ_T and θ_R, thus, $d\theta_T$ and $d\theta_R$ were set to the same value. Based on the above parameter settings, the estimation error of speed was calculated according to (16) with bistatic angles varying from 0° to 180°, the obtained overall absolute speed errors are illustrated as a red curve in Fig. 16(a). The reason why the estimation error is large when bistatic angle is too small or large is that the proposed vector velocity estimation method relies on the radial velocity V_R and elliptical velocity V_E. When the bistatic angle approaches 0°, the target may be located either at a far distance away from radars or at the extension line on one side of the baseline. When the bistatic angle approaches 180°, the target is located on the baseline. Under the above scenarios, the directions of two Doppler velocities will coincide, (12) no longer applies, so that large errors will appear. In practical target tracking applications, the task of HFSWR is to monitor distant targets within the radar detection area, the above situations seldom happen and are of little concern. Considering

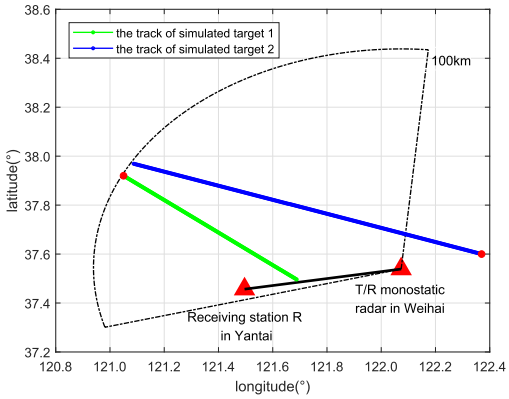

Fig. 17. Tracks of simulated target 1 and simulated target 2.

that the maximum detection range of the developed radar is 100 km, only a limited range of bistatic angles makes sense in practice. If the bistatic angles are restricted to be $\beta \in [5°, 155°]$, the corresponding absolute speed errors are depicted as a green curve in Fig. 16(a), which shows that the speed estimation errors are less than 3 km/h.

Then the estimation error of heading was calculated according to (19) with bistatic angles varying from 5° to 180°, the obtained absolute heading errors are illustrated in Fig. 16(b), which illustrates that the heading errors are around 2°.

C. Overall Effect of Bistatic Angle and Doppler Velocity on Estimation Errors

In real target tracking scenarios, vessels move following certain sea routines. The radial velocity V_R, elliptical velocity V_E, bistatic angle β all change as the vessel moves. In this section, the tracks of two simulated targets, named as target 1 and target 2, were used to evaluate the speed and heading estimation errors, as shown in Fig. 17. The red solid dots indicate the starting plots of the tracks. The positions of the T/R monostatic radar in Weihai and the receiving station R in Yantai are denoted with red solid triangles. The black line between them represents the baseline. Simulated target 1 and simulated target 2 move at a speed of 20 km/h with headings of 130°, 290°, and initial locations of (121.05°E, 37.92°N), (122.37°E, 37.6°N), respectively. The track of simulated target 1 consists of 220 plots, while the track of simulated target 2 contains 360 plots.

According to the above parameter settings, the radial velocities, elliptical velocities, and bistatic angles were calculated for two simulated targets, then (16) and (19) were applied to obtain the speed and heading estimation errors, which are shown in Fig. 18. The black arrows in Fig. 18(c) and (d) indicate the order in which the error values occur.

Fig. 18 demonstrates that although both targets move at the same speed, the absolute speed and heading errors are different due to different headings. The simulated target 1 moves from the far end to the baseline, its bistatic angle increases from 17° to nearly 180°. Fig. 18(a) and (b) demonstrates that when the bistatic angle is less than 160°, both the absolute speed errors and heading errors remain nearly constant with values of less

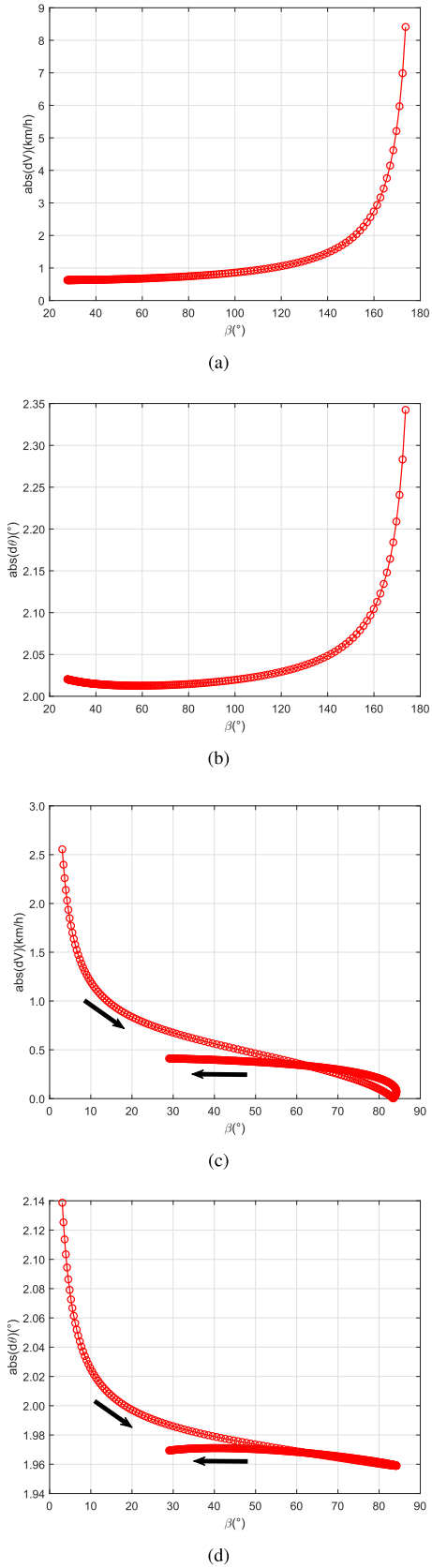

Fig. 18. Absolute estimation error of speed and heading for simulated target 1 and simulated target 2. (a) Absolute estimation error of speed for simulated target 1. (b) Absolute estimation error of heading for simulated target 1. (c) Absolute estimation error of speed for simulated target 2. (d) Absolute estimation error of heading for simulated target 2.

than 3 km/h, and 2.1°, respectively. However, when the bistatic angle exceeds 160°, both the speed and heading errors increase rapidly due to "baseline instability." The simulated target 2 moves from the Weihai radar side to the far end, its bistatic angle first increases from 3° to 84°, then decreases from 84° to 29°. Fig. 18(c) and (d) illustrates that the absolute speed errors are within 2.5 km/h, while the absolute heading errors are around 2°. With the increase of the bistatic angle, both speed and heading errors have descending trends. Moreover, it should also be noticed that the speed or heading estimation errors may be different even using the same bistatic angles. This is because the same bistatic angle may correspond to different positions, thus different Doppler velocities.

From the above experiments, it can be concluded that within a reasonable target detection area, the proposed method can provide accurate vector velocity estimation results. E.g., if the bistatic angle is within the range of [40° 60°], which is similar to those of two example targets, the absolute errors of speed and heading are about 0.5 km/h and 2°.

VI. Conclusion

In this article, the complementary target position information as well as the radial and elliptical Doppler velocities provided by a newly developed T/R-R composite compact HFSWR system are investigated and used to estimate the vessel vector velocity. First, two track sets obtained by T/R monostatic radar and T-R bistatic radar are associated and combined to produce fused tracks with improved positioning accuracy. Then the radial and elliptical Doppler velocities are combined by geometric manipulation to determine the vessel speed and heading, thus a vector velocity is achieved. Moreover, the estimation error of vessel speed and heading are analyzed both theoretically and experimentally. Experimental results from field data verify that the proposed method can estimate vessel vector velocity with relatively high accuracy, which enables the target tracking system to be capable of providing target speed and heading information. The estimated results can be further used to improve positioning accuracy.

Also, it should be noted that the track association and fusion procedure used in this article assume that both T/R and T-R radars acquire target measurements simultaneously. In practical applications, there exist some circumstances that one radar detects a target while the other one does not. Therefore, more efforts should be directed at investigating special track-to-track association and fusion methods to make them applicable to more general situations.

In future work, the estimated speed and heading may be further explored to improve the accuracy of state prediction and data association of target tracking algorithms.

References

[1] W. Huang, S. Wu, E. Gill, B. Wen, Z. Yang, and J. Hou, "HF radar wind and wave measurement over the Eastern China Sea," *IEEE Trans. Geosci. Remote Sens.*, vol. 40, no. 9, pp. 1950–1955, Sep. 2002.

[2] S. Maresca, P. Braca, J. Horstmann, and R. Grasso, "Maritime surveillance using multiple high-frequency surface-wave radars," *IEEE Trans. Geosci. Remote Sens.*, vol. 52, no. 8, pp. 5056–5071, Aug. 2014.

[3] J. Chen, D. Dao, and H. Chien, "Ship echo identification based on norm-constrained adaptive beamforming for an arrayed high-frequency coastal radar," *IEEE Trans. Geosci. Remote Sens.*, vol. 59, no. 2, pp. 1143–1153, Feb. 2021

[4] S. Park, C. J. Cho, B. Ku, S. Lee, and H. Ko, "Compact HF surface wave radar data generating simulator for ship detection and tracking," *IEEE Geosci. Remote Sens. Lett.*, vol. 14, no. 6, pp. 969–973, Jun. 2017.

[5] L. Chuang, Y.-J. Chung, and S. T. Tang, "A simple ship echo identification procedure with SeaSonde HF radar," *IEEE Geosci. Remote Sens. Lett.*, vol. 12, no. 12, pp. 2491–2495, Dec. 2015.

[6] H. J. Roarty, E. R. Lemus, E. Handel, S. M. Glenn, D. E. Barrick, and J. Isaacson, "Performance evaluation of SeaSonde high-frequency radar for vessel detection," *Mar. Technol. Soc. J.*, vol. 45, no. 3, pp. 14–24, 2011.

[7] Y. Lai, H. Zhou, Y. Zeng, and B. Wen, "Accuracy assessment of surface current velocities observed by OSMAR-S high-frequency radar system," *IEEE J. Ocean. Eng.*, vol. 43, no. 4, pp. 1068–1074, Oct. 2018.

[8] B. Lu, B. Wen, Y. Tian, and R. Wang, "A vessel detection method using compact-array HF radar," *IEEE Geosci. Remote Sens. Lett.*, vol. 14, no. 11, pp. 2017–2021, Nov. 2017.

[9] T. Helzel, B. Hansen, M. Kniephoff, L. Petersen, and M. Valentin, "Introduction of the compact HF radar WERA-S," in *Proc. IEEE/OES Baltic Int. Symp.*, Klaipeda, Lithuania, May 2012, pp. 1–3.

[10] Y. Ji, J. Zhang, Y. Wang, W. Sun, and M. Li, "Target monitoring using small-aperture compact high-frequency surface wave radar," *IEEE Aerosp. Electron Syst. Mag.*, vol. 33, no. 3, pp. 22–31, Mar. 2018.

[11] W. Sun, W. Huang, Y. Ji, Y. Dai, P. Ren, and P. Zhou, "Vessel tracking with small-aperture compact high-frequency surface wave radar," in *Proc. MTS/IEEE Oceans*, Marseille, France, Jun. 2019, pp. 1–4.

[12] W. Sun *et al.*, "A vessel azimuth and course joint re-estimation method for compact HFSWR," *IEEE Trans. Geosci. Remote Sens.*, vol. 58, no. 2, pp. 1041–1051, Feb. 2020.

[13] W. Huang, E. Gill, X. Wu, and L. Li, "Measurement of sea surface wind direction using bistatic high-frequency radar," *IEEE Trans. Geosci. Remote Sens.*, vol. 50, no. 10, pp. 4117–4122, Oct. 2012.

[14] R. L. Hardman, L. R. Wyatt, and C. C. Engleback, "Measuring the directional ocean spectrum from simulated bistatic HF radar data," *Remote Sens.*, vol. 12, 2020, Art. no. 313.

[15] W. Sun, M. Ji, W. Huang, Y. Ji, and Y. Dai, "Vessel tracking using bistatic compact HFSWR," *Remote Sens.*, vol. 12, no. 8, 2020, Art. no. 1266.

[16] S. Park, C. J. Cho, Y. Lee, A. D. Costa, S. Lee, and H. Ko, "Coastal ship monitoring based on multiple compact high frequency surface wave radars," in *Proc. IEEE Int. Conf. Multisensor Fusion Integr. Intell. Syst.*, Daegu, South Korea, Dec. 2017, pp. 565–569.

[17] P. Braca, S. Maresca, R. Grasso, K. Bryan, and J. Horstmann, "Maritime surveillance with multiple over-the-horizon HFSW radars: An overview of recent experimentation," *IEEE Aerosp. Electron Syst. Mag.*, vol. 30, no. 12, pp. 4–18, Dec. 2015.

[18] X. F. Ai, Y. Huang, F. Zhao, J. Yang, Y. Li, and S. Xiao, "Imaging of spinning targets via narrow-band T/R-R bistatic radars," *IEEE Geosci. Remote Sens. Lett.*, vol. 10, no. 2, pp. 362–366, Mar. 2013.

[19] S. Anderson, "Bistatic and stereoscopic configurations for HF radar," *Remote Sens.*, vol. 12, no. 4,2020, Art. no. 689.

[20] K. Zhao, C. Yu, and G. Zhou, "Simultaneous target flying mode identification and altitude estimation in bistatic T/R-R HFSWR," *Asian J. Control*, vol. 18, no. 3, pp. 1062–1074, 2016

[21] R. Wang, B. Wen, and W. Huang, "A support vector regression based method for target direction of arrival estimation from HF radar data," *IEEE Geosci. Remote Sens. Lett.*, vol. 15, no. 5, pp. 674–678, May 2018.

[22] G. Vivone, P. Braca, and J. Horstmann, "Knowledge-based multi-target ship tracking for HF surface wave radar systems," *IEEE Trans. Geosci. Remote Sens.*, vol. 53, no. 7, pp. 3931–3949, Jul. 2015.

[23] D. Nikolić *et al.*, "Multi-radar multi-target tracking algorithm for maritime surveillance at OTH distances," in *Proc. Int. Radar Symp.*, Krakow, Poland, 2016, pp. 1–6.

[24] O. Nova, C. Guiffaut, and A. Reineix, "Method for the sea clutter characterization in HF surface wave radars from the fields diffracted by the sea surface," *IEEE J. Sel. Topics Appl. Earth Observ. Remote Sens.*, vol. 13, pp. 403–413, Jan. 2020.

[25] Y. J. Chung, L. Z. H. Chuang, Y. R. Chen, Y. J. Yang, and I. Tsui, "Characteristic investigation of ionospheric clutter of a coastal high-frequency radar," in *Proc. MTS/IEEE Oceans*, Kobe, Japan, 2018, pp. 1–4.

[26] M. Eslami Nazari, W. Huang, and C. Zhao, "Radio frequency interference suppression for HF surface wave radar using CEMD and temporal windowing methods," *IEEE Geosci. Remote Sens. Lett.*, vol. 17, no. 2, pp. 212–216, Feb. 2020.

[27] A. F. García-Fernández, A. S. Rahmathullah, and L. Svensson, "A metric on the space of finite sets of trajectories for evaluation of multi-target tracking algorithms," *IEEE Trans. Signal Process.*, vol. 68, pp. 3917–3928, Jun. 2020.
[28] R. Singer and A. Kanyuck, "Computer control of multiple site track correlation," *Automatica*, vol. 7, no. 4, pp. 455–463, 1971.
[29] S. He, H. Shin, and A. Tsourdos, "Joint probabilistic data association filter with unknown detection probability and clutter rate," *Sensors*, vol. 18, no. 1,2018, Art. no. 269.
[30] S. P. Coraluppi and C. A. Carthel, "Multiple-hypothesis tracking for targets producing multiple measurements," *IEEE Trans. Aerosp. Electron. Syst.*, vol. 54, no. 3, pp. 1485–1498, Jun. 2018.
[31] A. M. Aziz, "A new fuzzy clustering approach for data association and track fusion in multisensor-multitarget environment," in *Proc. IEEE Aerosp. Conf.*, Big Sky, MT, USA, 2011, pp. 1–10.
[32] A. M. Aziz, "Fuzzy track-to-track association and track fusion approach in distributed multisensor-multitarget multiple-attribute environment," *Signal Process.*, vol. 87, no. 6, pp. 1474–1492, 2007.
[33] Z. Zhang and C. Chen, "Feature-weighted track-to-track association based on adaptive fuzzy C-shell cluster," in *Proc. Int. Conf. Intell. Control Inf. Process.*, Wuhan, China, 2015, pp. 161–165.
[34] M. Nazari, S. Pashazadeh, and L. Mohammad-Khanli, "An adaptive density-based fuzzy clustering track association for distributed tracking system," *IEEE Access*, vol. 7, pp. 135972–135981, 2019.
[35] W. Du, H. Ning, Y. Wei, and J. Wang, "Fuzzy double-threshold track association algorithm using adaptive threshold in distributed multisensor-multitarget tracking systems," in *Proc. IEEE Int. Conf. Green Comput. Commun.*, Beijing, China, 2013, pp. 1133–1137.
[36] W. Kazimierski, "Verification of neural approach to radar-AIS tracks association for maneuvering targets based on kinematic spatial information," in *Proc. Int. Radar Symp.*, 2017, pp. 1–10.
[37] L. Zhang, D. Mao, J. Niu, Q. Wu, and Y. Ji, "Continuous tracking of targets for stereoscopic HFSWR based on IMM filtering combined with ELM," *Remote Sens.*, vol. 12, no. 2, 2020, Art. no. 272.
[38] J. Ajgl and O. Straka, "Covariance intersection in track-to-track fusion: Comparison of fusion configurations," *IEEE Trans. Ind. Inf.*, vol. 14, no. 3, pp. 1127–1136, Mar. 2018.
[39] S. Mori, W. H. Barker, C. Y. Chong, and K. C. Chang, "Track association and track fusion with nondeterministic target dynamics," *IEEE Trans. Aerosp. Electron. Syst.*, vol. 38, no. 2, pp. 659–668, Apr. 2002.
[40] Y. Shi, K. Zhang, T. Zhang, N. Lin, Y. Zhao, and Y. Zhao, "An adaptive track fusion approach with fuzzy computation for multi-sensor," in *Proc. Int. Conf. Smart Internet Things*, Xi'an, China, 2018, pp. 245–249.
[41] K. C. Chang, Z. Tian, and S. Mori, "Performance evaluation for MAP state estimate fusion," *IEEE Trans. Aerosp. Electron. Syst.*, vol. 40, no. 2, pp. 706–714, Apr. 2004.
[42] A. K. Singh and N. Sood, "Modelling and simulation of multi-target multi-sensor data fusion for trajectory tracking," *Defence Sci. J.*, vol. 59, no. 3, pp. 205–214, 2009.
[43] S. Chen and W. Huang, "Maneuvering target tracking from nautical radar images using particle-Kalman filters," *J. Electromagnet. Wave*, vol. 27, no. 18, pp. 2366–2378, 2013.
[44] S. Bordonaro, P. Willett, and Y. Bar-Shalom, "Decorrelated unbiased converted measurement Kalman filter," *IEEE Aerosp. Electron. Syst. Mag.*, vol. 50, no. 2, pp. 1431–1444, Apr. 2014.

Weifeng Sun (Member, IEEE) received the B.Eng. degree in communication engineering and the Ph.D. degree in signal and information processing from Shandong University, Jinan, China, in 2005 and 2010, respectively.

He is currently an Associate Professor with the College of Oceanography and Space Informatics, China University of Petroleum (East China), Qingdao, China. From 2018 to 2019, he was a Visiting Scholar with the Memorial University of Newfoundland, St. John's, NL, Canada. His research interests include marine target detection and tracking via compact high-frequency surface wave radar, and image processing.

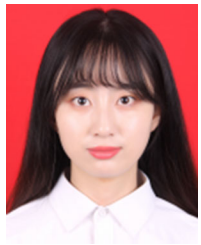

Zhenzhen Pang received the B.Eng. degree in measurement and control technology and instruments from Qufu Normal University, Rizhao, China, in 2019. She is currently working toward the M.Eng. degree with the College of Control Science and Engineering, China University of Petroleum (East China), Qingdao, China.

Her research interests includes target detection and tracking with T/R-R composite compact high-frequency surface wave radar.

Weimin Huang (Senior Member, IEEE) received the B.S., M.S., and Ph.D. degrees in radio physics from Wuhan University, Wuhan, China, in 1995, 1997, and 2001, respectively, and the M.Eng. degree in electrical engineering from the Memorial University of Newfoundland, St. John's, NL, Canada, in 2004.

From 2008 to 2010, he was a Design Engineer with Rutter Technologies, St. John's, NL, Canada. Since 2010, he has been with the Faculty of Engineering and Applied Science, Memorial University of Newfoundland, where he is currently a Professor. He has authored more than 250 research papers. His research interests include the mapping of oceanic surface parameters via high-frequency ground wave radar, *X*-band marine radar, and global navigation satellite systems.

Dr. Huang has been a Technical Program Committee Member. He served as a Technical Program Co-Chair of the IEEE Newfoundland Electrical and Computer Engineering Conference, in 2012 and 2013. He is currently an Area Editor for the IEEE CANADIAN JOURNAL OF ELECTRICAL AND COMPUTER ENGINEERING, an Associate Editor for IEEE ACCESS, and an Editorial Board Member of *Remote Sensing*, and a Guest Editor for IEEE JOURNAL OF SELECTED TOPICS IN APPLIED EARTH OBSERVATIONS AND REMOTE SENSING. He serves as a regular reviewer over 60 international journals and a reviewer for many IEEE international conferences, such as RadarCon, International Conference on Communications, IEEE Global Communications Conference, and IEEE Geoscience and Remote Sensing Society, and Oceans. He was the recipient of Postdoctoral Fellowship from Memorial University of Newfoundland. In 2017, he was the recipient of the Discovery Accelerator Supplements Award from the Natural Sciences and Engineering Research Council of Canada. He was the recipient of the IEEE Geoscience and Remote Sensing Society 2019 Letters Prize Paper Award.

Yonggang Ji (Member, IEEE) received the B.S. and M.S. degrees in electronic engineering from the Ocean University of China, Qingdao, China, in 2001 and 2003, respectively, and the Ph.D. degree in physical oceanography from the Institute of Oceanology, Chinese Academy of Sciences, Qingdao, China, in 2006.

He is currently a Professor with the College of Oceanography and Space Informatics, China University of Petroleum (East China), Qingdao, China. His research interests include high-frequency surface wave radar (HFSWR) and applications, compact high frequency over the horizon radar system, marine target monitoring with multiple remote sensors, remote sensing of sea state, and ocean remote sensing.

Yongshou Dai received the B.S. degree in production process automation from the University of Petroleum, Dongying, China, in 1986, the M.Eng. degree in computer application from Northern Jiaotong University, Beijing, China, in 1991, and the Ph.D. degree in control theory and control engineering from the University of Science and Technology Beijing, Beijing, China, in 2007.

He is currently a Professor with the College of Oceanography and Space Informatics, China University of Petroleum (East China), Qingdao, China. His research interests include seismic signal processing, marine environment monitoring, and information processing.